Interaction of Actin and ADP with the Head Domain of Smooth Muscle Myosin: Implications for Strain-Dependent ADP Release in Smooth Muscle[†]

Christine R. Cremo*[,‡] and Michael A. Geeves[§]

Department of Biochemistry and Biophysics, Washington State University, Pullman, Washington 99164, and Max-Planck-Institut für Molekulare Physiologie, Dortmund, Germany

Received September 9, 1997; Revised Manuscript Received December 10, 1997

ABSTRACT: Transient kinetic methods were used to study interactions between actin, MgADP, and smooth muscle (chicken gizzard) myosin subfragment 1 (smS1). The equilibrium dissociation constant (K_d) of actin for smS1 was 3.5 nM, tighter than that of skeletal S1 (skS1). Actin binding to smS1 was weakened 5-fold by saturation with ADP compared to 30−60-fold for skS1. The K_d of ADP for smS1 was increased from 1.2 to 5 μM by actin, whereas for skS1 values increased from 2 to 100 μM. Thus, coupling between ADP and actin binding is weaker for smS1. Previous studies show that release of ADP from actin·smS1·ADP produces a tilt of the regulatory domain [Whittaker, M., Wilson-Kubalek, E. M., Smith, J. E., Faust, L., Milligan, R. A., and Sweeney, H. L. (1995) *Nature 378*, 748−751]. This result was confirmed by independent structural methods; tilting was absent for skS1, and the K_d for ADP was in agreement with the values measured here [Gollub, J., Cremo, C. R., and Cooke, R. (1996) *Nat. Struct. Biol. 3*, 796−802; Poole, K. I. V., Lorenz, M., Ellison, P., Evans, G., Rosenbaum, G., Boesecke, P., Holmes, K. C., and Cremo, C. R. (1997) *J. Muscle Res. Cell Motility 18*, 264]. We discuss tilting upon ADP release with respect to our measurements, previous measurements with skS1, and nucleotide concentrations in smooth muscle. We propose that these data suggest a strain-dependent ADP release mechanism that may be accentuated in smooth muscles.

The ATP-driven cyclic interaction of myosin heads (S1)[1] with actin provides the molecular basis of muscle contraction. Most of the detailed characterization of the properties of S1 in solution have used fast skeletal muscle myosin II, but studies of other muscle and nonmuscle myosins show that they follow the same basic kinetic mechanism (Schemes 1 and 2). This applies to myosin II from vertebrate smooth muscles (*1*). However, the rate and equilibrium constants for individual steps (*2*) and the duty ratio (*3*) are different from the skeletal isoform. These factors are thought to reflect the different biological functions of the two muscle types (*4*, *5*) and the underlying differences in the shortening velocity and the economy of force production.

In addition to the kinetic differences between the smooth and skeletal isoforms, it has recently become apparent that there may also be important structural differences. Three-dimensional density maps of both nucleotide-free (rigor) and the MgADP-bound states of the chicken gizzard S1 (smS1) bound to F-actin have been obtained using cryo-electron microscopy coupled with helical image analysis and averaging (*6*). They found a 23° tilt of the regulatory domain of smS1 upon ADP release. This finding was unexpected because ADP-induced structural changes in skeletal muscle myosin have not been found despite the use of several methods [summarized in (*7*)]. A direct comparison between smooth and skeletal isoforms using EPR spectroscopy showed that indeed an angle change similar to that found by Whittaker et al. (*6*) was unique to the smooth muscle isoform (*8*). And this was confirmed in a preliminary report using X-ray fiber diffraction methods (*9*). Together these three reports provide compelling evidence that MgADP release may be associated with a motion of the regulatory domain of smooth muscle myosin and that smooth muscle myosin has an extra component of tilting in the direction of force generation. These studies raise interesting questions about the role of this motion in the powerstroke and in myosin-linked regulation (smooth muscle myosin, unlike the skeletal isoform, is a highly regulated motor). The differences between the MgADP and the rigor structural states in smooth muscle S1 are of particular interest when considering the role of MgADP in the force maintenance in smooth muscle (see Discussion).

Despite the interesting effects of ADP upon the structure of smooth muscle myosin, the solution kinetics of the interaction of ADP with smooth muscle acto−myosin and the respective protein subfragments have not been studied in detail. Several investigators have made important kinetic and equilibrium measurements of smS1 (*2*, *4*, *10*, *11*).

[†] This work was supported by grants from the National American Heart Association and its Washington State affiliate (C.R.C.), and the National Institutes of Health, NIAMS (C.R.C., AR 40917).

* Corresponding author. Telephone: 509 335 2428. Fax: 509 335 9688. Email: cremo@wsu.edu.

[‡] Washington State University.

[§] Max-Planck-Institut für Molekulare Physiologie.

[1] Abbreviations: S1, myosin subfragment 1; smS1 and skS1, S1 from smooth and skeletal muscle, respectively; V8, protease from *Staphylococus aureus*; mantADP/ATP, 2′(3′)-O-(*N*-methylanthraniloyl)-ADP/ATP; pyr-actin, actin labeled with pyrene iodoacetamide on Cys-374.

S0006-2960(97)02240-X CCC: $15.00
Published on Web 01/30/1998

However, taken together, these studies do not provide a sufficient characterization of the interaction of ADP with smooth muscle S1 to interpret the structural results.

We report here a detailed solution study of the interaction of ADP and actin with smS1 from chicken gizzard myosin. SmS1 was prepared by digestion of myosin with the *Staphylococcus aureus* protease (V8) and contains an intact head domain that is not regulated by phosphorylation (*12*). Gizzard is an extensively studied source of phasic muscle and is the source of protein in the structural studies mentioned above (*6*, *8*, *9*).

In summary, we find that the equilibrium dissociation constant for acto·S1 binding to ADP is 5 μM, in good agreement with the estimations from orientational changes in the regulatory domain (*8*, *9*). In the absence of actin, the binding of ADP is similar, tighter by only a factor of ~5. This is a small magnitude for the thermodynamic coupling between actin binding and ADP binding compared to a value of 30−60 for skeletal muscle S1. Thermodynamic arguments suggest that the structural change associated with ADP release is unlikely to be useful for force generation, but we propose that it could be a mechanism to extend the average lifetime of strain-bearing crossbridges by limiting the rate of ADP release from strain-bearing crossbridges.

MATERIALS AND METHODS

Smooth muscle myosin was purified (*13*) from chicken gizzards that had been cleaned and frozen in liquid nitrogen prior to storage at −80 °C (obtained from Pell-Freeze). Myosin was used immediately to prepare S1 by digestion with *Staphylococcus aureus* protease [V8 protease; Sigma or ICN; (*12*)]. S1 was pooled from the gel filtration column, precipitated by addition of 2.5 volumes of saturated ammonium sulfate, dialyzed to 10 mM MOPS, pH 7.0, 0.1 mM EGTA, 1 mM DTT, and clarified by ultracentrifugation prior to use in kinetic experiments. The molar concentration was determined by the absorbance at 280 nm using an extinction coefficient of E (0.1%) = 0.75 cm^{-1} and a molecular mass of 130 000 daltons. Native gel analysis (*14*) showed that the preparation did not contain detectable levels of HMM or myosin, but contained small amounts of S2 fragments. Steady-state NH_4-EDTA and K^+-ATPase values (*15*), respectively, were 3.3 and 1.9 μmol min^{-1} mg^{-1}.

Rabbit skeletal muscle actin was prepared by the method of (*16*) and labeled with pyrene at cys-374 as described (*17*). MantADP was synthesized as described (*18*).

All kinetic experiments were performed at 20 °C in 20 mM MOPS, pH 7, 0.1 M KCl, 1 mM DTT, 0.1 mM EGTA, 5 mM $MgCl_2$ with a standard Hi-Tech SF61MX stopped-flow spectrophotometer using a 100 W Xe/Hg lamp and a monochromator for wavelength selection. For 90° light scattering experiments, the excitation wavelength was 400 nm, and the emission path was unobstructed. Tryptophan fluorescence was excited at 295 nm and emission detected after passing through a WG 320 cutoff filter (Schott, Mainz). Pyrene and mantADP fluorescence was excited at 365 nm and emission detected after passing through a KV 389-nm cutoff filter (Schott, Mainz). All of the transients shown are the average of 3−5 shots of the stopped-flow apparatus, and the best fit to a single or double exponential function is shown superimposed.

Scheme 1

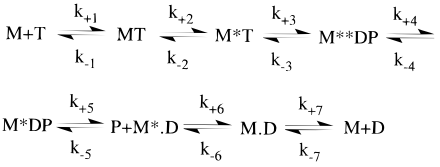

Scheme 2

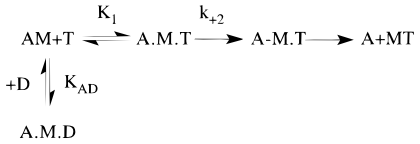

Scheme 3

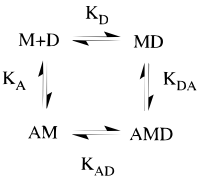

Scheme 4: Complexes of Pyr-actin and MantADP with S1 and Relative Intensities of Their MantADP and Pyr-actin Fluorescence (Fl) Signals

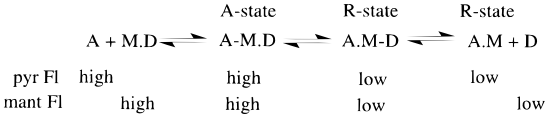

Interpretation of Kinetic Data. We interpret the kinetics of ATP interacting with S1 in terms of the well-established seven-step model (*19*) shown in Scheme 1, where k_{+i}, k_{-i}, and K_i (k_{+i}/k_{-i}) are the forward and reverse rate constants and the equilibrium constant of the ith step of the reaction. ATP binds rapidly to S1 (or M) in a two-step reaction [rapid equilibrium binding (1) followed by a fast almost irreversible step (2)]. ATP is then reversibly hydrolyzed on the protein (3), and the following rate limiting conformational change (4) limits phosphate release and the faster two-step ADP release (6 and 7). Asterisks refer to complexes with enhanced protein fluorescence.

We investigated the ATP-induced dissociation of acto·S1 and the inhibition of the ATP reaction by ADP and have interpreted the data in terms of the models developed by Millar and Geeves (*20*) and Siemankowski and White (*21*).

In Scheme 2, ATP binds rapidly and reversibly to acto·S1 (K_1) and is followed by a rate-limiting isomerization ($\mathbf{k}_{+2}$) of the complex which leads to rapid dissociation of actin. ADP competes with ATP for the nucleotide binding site on acto·S1.

Each of the complexes in Scheme 1 can bind to actin (A), and at least two acto·S1 nucleotide states exist for each nucleotide state [R-state and A-state; see Scheme 4 (*22*, *23*)]. However, for the current studies, a simpler model will suffice. We have examined the binding of smS1 and smS1·ADP to actin and interpret the data in terms of a single-step binding model as shown in Scheme 3. Scheme 3 [based on (*21*)] also shows the relationship between actin and ADP binding to S1. Note that in Scheme 3 the equilibrium constants are defined as dissociation constants ($K_i = k_{-i}/k_{+i}$) and that K_D

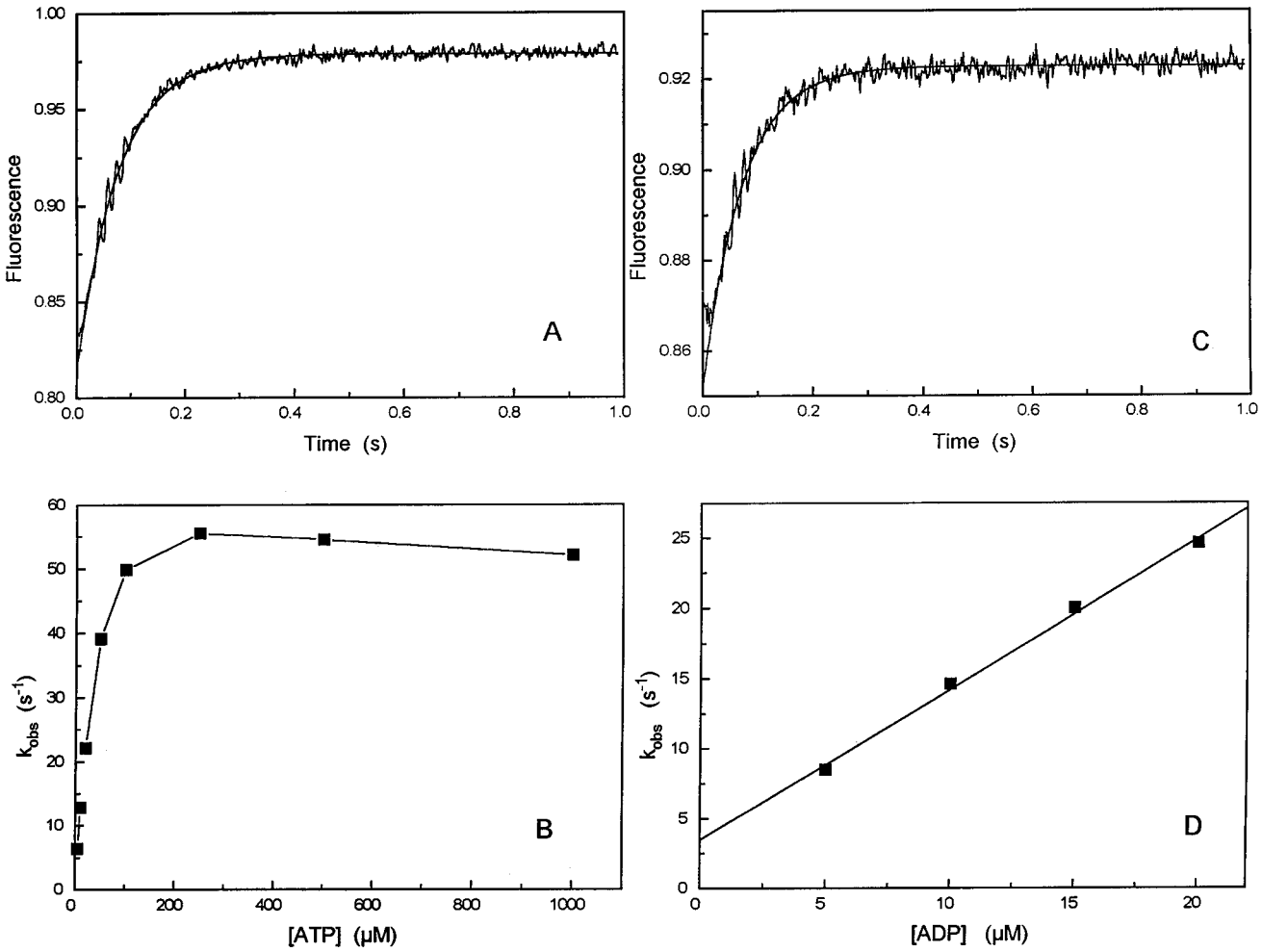

FIGURE 1: Rate of association of ATP and ADP with smS1. (A) The protein fluorescence changes observed on mixing 0.5 μM smS1 with 10 μM ATP. The best-fit single exponential is superimposed with k_{obs} = 12.8 s^{-1} amp + 16%. (B) The dependence of k_{obs} on [ATP]. At low concentrations, the data fit a straight line with slope (K_1k_{+2}) 2.1 × 10^6 M^{-1} s^{-1}. At high concentrations, k_{obs} saturates at a value of ~50 s^{-1}. (C) The protein fluorescence change observed on mixing 5 μM ADP with 0.5 μM smS1. The best-fit single exponential is superimposed with k_{obs} = 14.6 s^{-1} amp + 7.3%. (D) The dependence of k_{obs} on [ADP]. The data fit a straight line with slope (k_{-6}/K_7) 1.1 × 10^6 M^{-1} s^{-1} and intercept (k_{+6}) of 3.5 s^{-1}. Reaction conditions: 0.1 M KCl, 1 mM DTT, 0.1 mM EGTA, 5 mM $MgCl_2$, 20 mM MOPS, pH 7.0, 20 °C.

is equivalent to $1/K_6K_7$ ($k_{-D} = k_{+6}$, $k_{+D} = K_7k_{+6}$) in Scheme 1.

RESULTS

The binding of nucleotide to S1 is conveniently followed by the increase in protein fluorescence associated with nucleotide binding (*2*, *19*, *24*). Figure 1A shows the fluorescence change observed on rapidly mixing 10 μM ATP with 0.5 μM smS1. The transient increase in fluorescence was well described by a single exponential with k_{obs} = 12.8 s^{-1} and an amplitude of +16%. The dependence of k_{obs} on ATP concentration (Figure 1B) was linear up to about 100 μM ATP (slope = K_1k_{+2} = 2.1 × 10^6 M^{-1} s^{-1}; see Scheme 1) and then appears to saturate at a value of 50 s^{-1}. The amplitude of the transient was constant up to 100 μM ATP and then declined to a value of 11% at 1 mM ATP (data not shown). This pattern of k_{obs} and amplitude dependence on [ATP] is well established for myosins and suggests that as for skeletal myosin subfragment 1 (skS1) there are two fluorescence changes associated with the ATP reaction: a fluorescence increase of 7−10% on ATP binding followed by a further increase of 5−7% on ATP hydrolysis (Scheme 1). Marston and Taylor (*2*) established by quenched-flow studies that for smS1 at low ionic strength the rate of ATP cleavage ($k_{+3} + k_{-3}$) correlates with the maximum k_{obs} of the fluorescence change.

The same reaction was also studied for ADP binding, and the results are shown in Figure 1C,D. Again, a fluorescence increase was observed but smaller (~7%) than seen for ATP (16%), and this small amplitude restricted the range of ADP concentrations over which the data could be collected. Over the range 5−20 μM ADP the amplitude increased from 6 to 9% compatible with a relatively weak affinity of ADP for S1 (> 1 μM) and k_{obs} was linearly dependent on ADP concentration. The slope of the plot of k_{obs} vs [ADP] (Figure 1D) defines the second order rate constant of ADP binding (k_{+D} or k_{-6}/K_7 = 1.1 × 10^6 $M^{-1}s^{-1}$) which is similar to that of ATP. The intercept is not well defined by these data but suggests a value of k_{-D} or k_{+6} of 3.5 s^{-1}.

The binding of ATP to smS1 produces a larger fluorescence increase than the binding of ADP (Figure 1); therefore, the displacement of ADP by ATP can be followed from the net increase in fluorescence. Figure 2A shows the reaction observed on adding 100 μM ATP to 0.5 μM smS1 in the

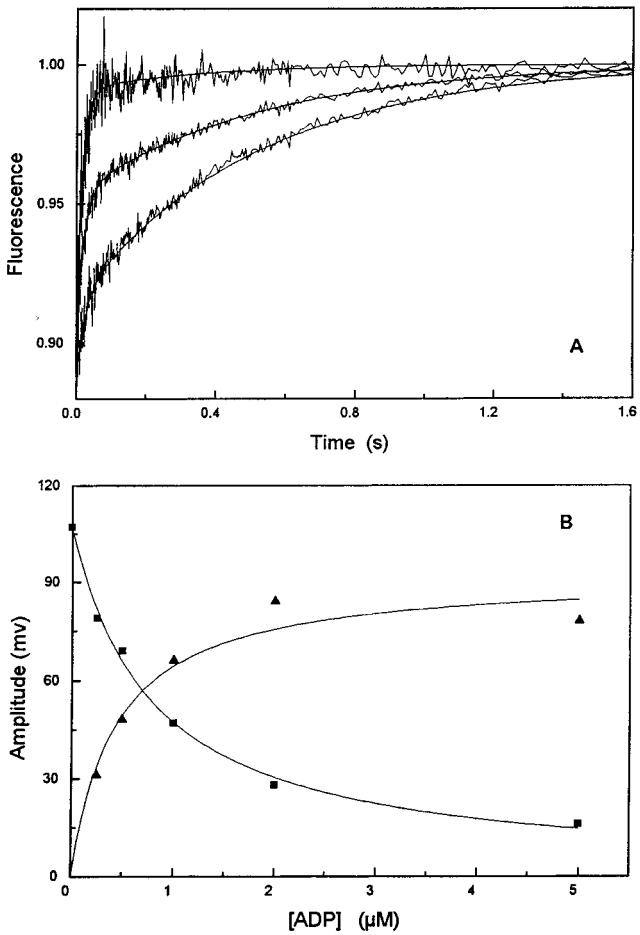

FIGURE 2: Displacement of ADP from smS1·ADP by addition of excess ATP. (A)The protein fluorescence changes observed on mixing 100 μM ATP with 0.5 μM smS1 and 0, 1.0, or 5.0 μM ADP. The best fit to a sum of two exponentials is superimposed. The k_{obs} values for the fast phases were 60.9 and 52.7 s^{-1} and too small an amplitude to measure and for the slow phases, too small to measure and 1.9 and 1.9 s^{-1}. (B) The dependence of the amplitudes of the two exponentials on ADP concentration. The data are fitted to a hyperbola with a K_d of 0.84 and 1.59 μM with maximum amplitudes of 91 and 108 mV for the slow (▲) and fast phase (■) respectively.

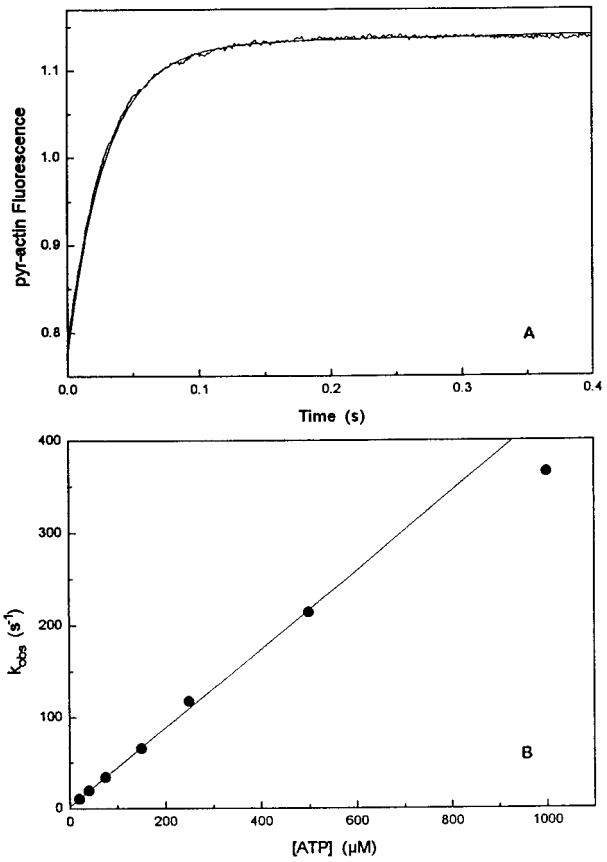

FIGURE 3: ATP-induced dissociation of pyr-acto·S1. (A) Observed pyrene fluorescence changes on addition of 50 μM ATP to 0.25 μM pyr-acto·S1. $k_{obs} = 32.2$ s^{-1}. (B) k_{obs} vs [ATP]. The slope of the best-fit line defines the apparent second-order rate constant, $(K_1k_{+2}) = 0.47 \times 10^6$ M^{-1} s^{-1}.

presence of 0, 1.0, or 5.0 μM ADP. On this extended time scale, the reaction is seen to be biphasic. The reaction could be described by the sum of two exponentials with k_{obs} of 61 and 1.9 s^{-1}, respectively. These values were relatively independent of [ADP] (ranges were $\pm$15 and $\pm$0.2 s^{-1}, respectively). The large variations in k_{obs} were mainly due to the problem of measuring the k_{obs} for processes with small amplitudes (particularly true for the minor components at the extremes of ADP concentrations). The amplitudes were dependent upon [ADP] with the fast phase decreasing and the slow phase increasing as [ADP] was increased (Figure 2B). This pattern of behavior is compatible with a simple model where the fast phase is the rate at which ATP binds to any unliganded S1 (at a k_{obs} defined by Figure 1b) and the slow process is the rate at which ATP replaces ADP from S1·ADP. Thus, k_{obs} of the slow phase is the rate at which ADP dissociates from S1 (k_{-D}, Scheme 3; or k_{+6}, Scheme 1), and it was independent of the concentration of ATP used (data not shown). The [ADP] dependence of the amplitudes was described by hyperbolas with best-fit dissociation constants of 0.89 and 1.6 μM for the fast and slow phases, respectively, which defines the equilibrium constant of ADP binding to S1 ($K_D = 1.2$ μM). The value of k_{obs} for the slow phase defines the rate constant of ADP dissociation (k_{-D} or k_{+6}) as 1.9 s^{-1}. The ratio calculated from Figure 1D and Figure 2A for k_{-D}/k_{+D} is 1.8 μM, in good agreement with the value of K_D from Figure 2b (1.2 μM).

Marston and Taylor (*2*) defined the rate of ATP-induced dissociation of acto·smS1 and showed that at ATP concentrations up to 5 mM, k_{obs} was hyperbolically dependent on ATP concentrations. This measurement was repeated at the more physiological ionic strengths as this reaction would be used to evaluate ADP binding to acto·S1 and the affinity of S1 for actin. We observed similar data to Marston and Taylor as shown in Figure 3A,B except that under our conditions little deviation from a linear dependence of k_{obs} on [ATP] was observed up to 500 μM ATP. The apparent second-order rate constant for ATP binding ($\mathbf{K_1k_{+2}}$) was 4.7 $\times 10^5$ M^{-1} s^{-1}, significantly slower than that reported by Marston and Taylor at lower ionic strength (2×10^6 M^{-1} s^{-1}). These data suggest that if the reaction saturates (as observed for all other S1's studied), then k_{max} is >600 s^{-1} under these conditions, consistent with the estimated value of 1300 s^{-1} from Marston and Taylor (*2*).

A similar approach to that taken to examine ADP displacement from smS1 was used with acto·smS1. ADP binding to acto·smS1 caused little dissociation of actin from the complex (K_d for actin <0.1 μM; see below), so the complex only dissociates on ATP binding. Figure 4 shows

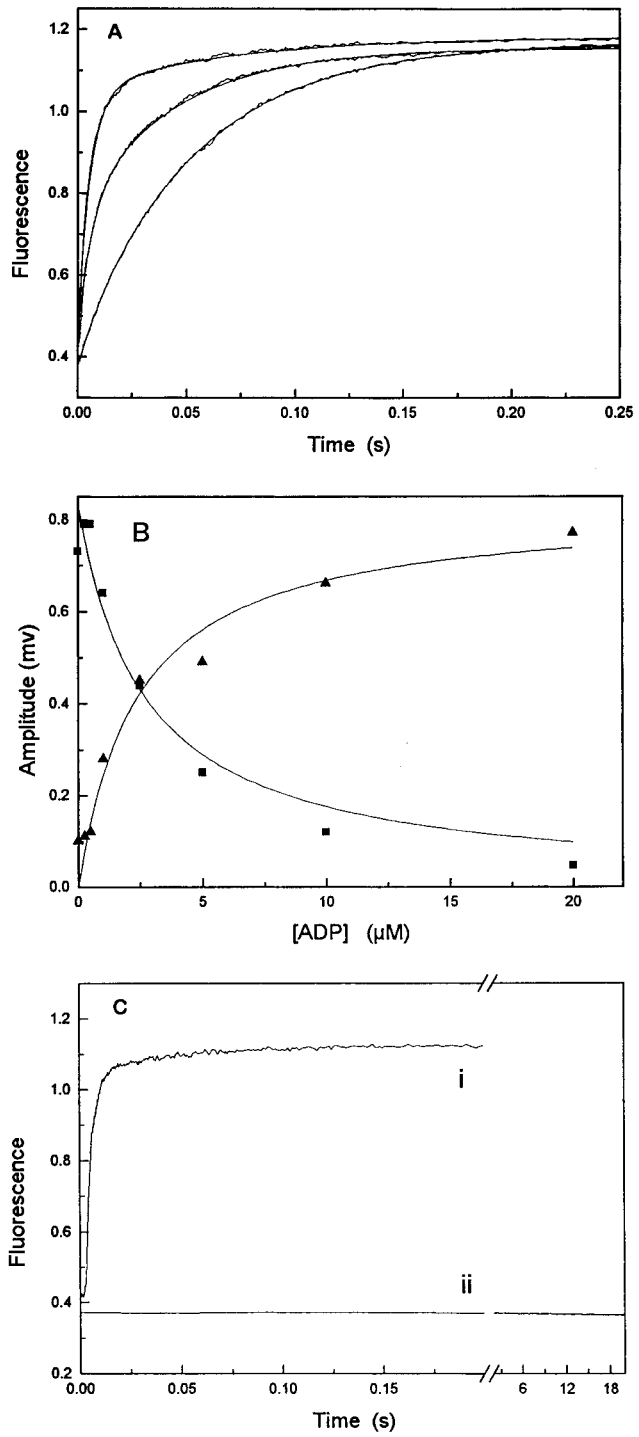

FIGURE 4: ADP inhibition of ATP-induced dissociation of pyr-acto·S1. (A) Observed fluorescence change on mixing 200 μM ATP with 0.5 μM pyr-acto·S1 and 0.25, 2.0, and 20 μM ADP. The best fit to the sum of two exponentials is superimposed with k_{obs} values for the fast phase, 175 and 167 s^{-1} and too small an amplitude to measure, and for the slow phase too small to measure and 22.6 and 18 s^{-1}, respectively. (B) [ADP] dependence of the observed amplitudes of the dissociation reaction. The best fits to hyperbola are superimposed and give K_d values of 4.7 and 5.3 μM for the slow (▲) and fast (■) phases, respectively. (C) Pyrene fluorescence changes on adding 1 mM ATP to 25 μM ADP, 0.5 μM pyr·actin, and 1 μM S1 (i) or 25 μM ADP to 0.5 μM pyr·actin and 1 μM S1(ii).

the transient observed on adding 200 μM ATP to 0.5 μM pyr-acto·smS1 in the presence of 0.25, 2.0, and 20 μM ADP. The transients were clearly biphasic with the fast phase decreasing and the slow phase increasing in amplitude as the ADP concentration increased (Figure 4B). The total amplitude remained constant, compatible with little dissociation of actin by ADP. The amplitude dependence could be described by hyperbolae with K_d of 4.7 and 5.3 μM. The k_{obs} for the reaction was 235 s^{-1} in the absence of ADP and decreased to ~170 s^{-1} at 20 μM ADP while k_{obs} for the slow phase was 22 s^{-1} at the lowest ADP where it could be reliably estimated and 18 s^{-1} at 20 μM ADP. This is compatible with a simple one step binding of ADP to acto·S1 with a K_{AD} (Scheme 3) of 5 μM and an ADP dissociation rate constant (k_{-AD}) of 22 s^{-1}. The decrease in k_{obs} for both phases is compatible with the competition between ATP and the free ADP for sites on acto·S1. A K_{AD} of 5 μM and a dissociation rate constant (k_{-AD}) of 22 s^{-1} predict an association rate constant for ADP of $k_{+AD} = k_{-AD}/K_{AD} = 4.4 \times 10^6$ M^{-1} s^{-1}.

The high affinity of ADP for acto·S1 suggests that the nature of the ADP binding is different in smS1 compared to skS1. One interpretation is that there is a greater occupancy of the A-state (in which ADP is tightly bound and actin weakly bound; see Scheme 4). To test this, 25 μM ADP was added to 0.5 μM pyr-actin and 1 μM S1, and as shown in Figure 4C curve ii, no detectable change in pyrene fluorescence was observed. Yet addition of 1 mM ATP to the ternary mixture (pyr-actin, S1, and ADP) at the same concentrations showed only a single exponential process of actin dissociation at the rate of ADP release from pyr-acto·S1·ADP (Figure 4C, curve i) showing that all of the acto·S1 had ADP bound in the active site. Thus, all of the pyr-acto·S1 binds ADP without inducing a change in the pyrene fluorescence. From this analysis, there is no detectable level of the A-state, and all of the actin in the acto·S1·ADP complex is tightly bound with the pyrene fluorescence quenched. A similar experiment with skS1 identifies 10% of the complex in the A-state (*25, 26*).

The data of Figures 2 and 4 suggest that the presence of actin on S1 reduces the affinity of S1 for ADP from 1.2 to 5 μM (the ratio, $K_{AD}/K_D = 4.2$, is the thermodynamic coupling constant; see Scheme 3 and Table 2) while the rate of ADP release was accelerated from 1.9 to 22 s^{-1}. Thus, there is a greater effect of actin on the rate of ADP release than

Table 1: Rate and Equilibrium Constants for the Interaction of SmS1 with Nucleotides According to Schemes 1 and 2

constant	units	value
K_1k_{+2}	M^{-1} s^{-1}	2.1×10^6
$k_3 + k_{-3}$	s^{-1}	50
k_{+6} (k_{-D})	s^{-1}	1.9
k_{-6}/K_7 (k_{+D})	M^{-1} s^{-1}	1.1×10^6
$\mathbf{K_1k_{+2}}$ (Scheme 2)	M^{-1} s^{-1}	0.47×10^6

Table 2: Rate and Equilibrium Constants Associated with Scheme 3 for ADP and MantADP[a]

step (n)	k_{+n} association rate constant (M^{-1} s^{-1})	k_{-n} dissociation rate constant (s^{-1})	K_n equilibrium constant (μM)
A	1.24×10^6	0.004[b]	0.0035
DA	0.23×10^6	0.0035[b]	0.024
AD	4.4[b] (3.6) $\times 10^6$	22 (25)	5.0 (7.0)
D	1.1 (2.0) $\times 10^6$	1.9 (0.13)	1.2 (0.075)

[a] Data in parenthesis are the values for mantADP. [b] Value calculated from the other two constants.

Table 3: Comparison of Equilibrium Dissociation Constants (in Molar Units) for the Head Fragments of Different Myosins (see Scheme 3)

	rab skel S1[a]	smS1[b]	cardiac S1[c]	dicty M864[d]
constant				
K_D	2.0×10^{-6}	1.2×10^{-6}	3.3×10^{-7}	3.7×10^{-5}
K_A	3.3×10^{-8}	3.5×10^{-9}	6.3×10^{-9}	7.1×10^{-8}
K_{DA}	1×10^{-6}	2.4×10^{-8}	1×10^{-7}	2×10^{-7}
K_{AD}	1.2×10^{-4}	5×10^{-6}	6.7×10^{-6}	9.4×10^{-5}
thermodynamic coupling				
$K_{DA}/K_A = K_{AD}/K_D$	30−60	4.2	15−20	2.8
acceleration				
k_{-AD}/k_{-D}	250	11.5	130	nd

[a] Rabbit skeletal chymotryptic S1 (*30*). [b] This study, chicken gizzard S1. [c] Bovine cardiac chymotryptic S1 (*21*). [d] *Dictyostelium discoideum* full-length myosin II head fragment (*30*).

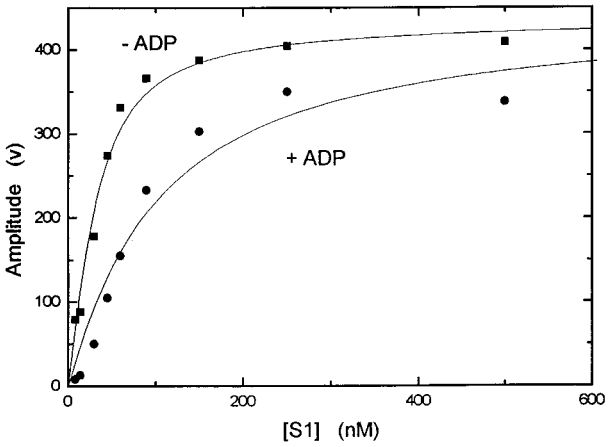

FIGURE 5: Affinity of pyr-actin for S1 in the presence and absence of ADP. 10 μM ATP was mixed with 30 nM phalloidin-stabilized pyr-actin and various S1 concentrations. The amplitude of the ATP-induced dissociation reaction is plotted as a function of S1 concentration, and the data are analyzed as a titration curve (the actin concentration was fixed at 30 nM, and the final amplitude was free to float) to give the affinity of actin for S1 as 16.5 nM and 87 nM in the absence and presence of 50 μM ADP, respectively. Adsorption of protein to the sufaces does not appear to be a problem down to concentrations of 1 nM (*27*). Conditions: as for Figure 1 but 0.2 M KCl.

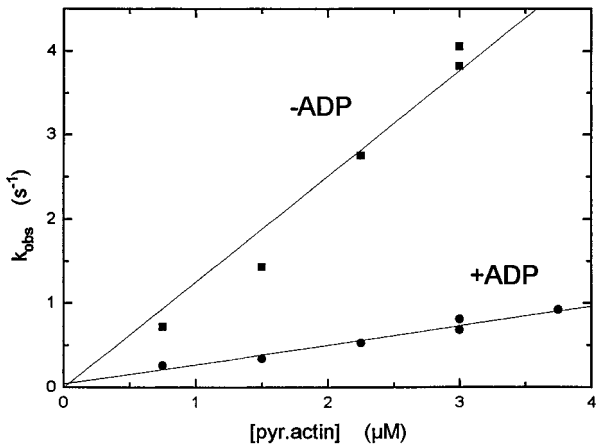

FIGURE 6: Rate of S1 binding to pyr-actin in the presence and absence of ADP. 0.25 μM smS1 was mixed with various concentrations of pyr·actin and the observed fluorescence transient fitted to a single exponential. Plot of k_{obs} vs pyr·actin in the absence and presence of 25 μM ADP gave slopes of 1.24 and 0.23×10^6 M^{-1} s^{-1}, respectively. The intercepts were not significantly different from zero.

on the affinity. These results contrast with those from fast skS1 in which the affinity and the dissociation rate constant are increased ~60- and 250-fold, respectively (Table 3).

To confirm the small thermodynamic coupling between actin and ADP binding to S1, we examined the affinity of S1 for actin in the presence and absence of ADP. The approach was that developed by Kurzawa and Geeves (*27*) which is a fluorescence titration of pyr-actin with S1 in the stopped-flow fluorometer (Figure 5). Phalloidin-stabilized pyr-actin (30 nM) and various concentrations of S1 were mixed with 10 μM ATP, and the amplitude of the observed dissociation reaction was used to estimate the fraction of actin bound to S1. At all concentrations of S1, the k_{obs} was 10 s^{-1}, and the amplitude increased hyperbolically with S1 concentration both in the absence of ADP and in the presence of 50 μM ADP. The best fit to the titration gave a K_d of 3.5 and 24 nM in the presence and absence of ADP, respectively (Table 2). As an affinity of 3.5 nM is difficult to measure with any precision, the experiment was repeated at 0.2 M KCl (data shown in Figure 5) and gave $K_A = 16.5$ nM and $K_{DA} = 87$ nM. Thus, at both salt concentrations, ADP reduced the affinity of smS1 for actin by 5−6-fold, which is similar to the reduction in ADP affinity for S1 caused by actin (5-fold).

To complete the study of actin and ADP interacting with S1, the influence of ADP on the rate of pyr-actin binding to S1 was measured. Addition of an excess of pyr-actin to 0.25 μM smS1 resulted in an exponential decrease in pyrene fluorescence, and the fitted values of k_{obs} are shown plotted against pyr-actin concentration in Figure 6. The slopes of the plots define the association rate constants k_{+A} and k_{+DA} and are listed in Table 2. The presence of ADP reduced the association rate constant of actin by a factor of 5, much smaller than that seen for skS1 which can be as much as 20-fold reduced by ADP (*25*).

The fluorescence of mant·ADP is enhanced 2−2.2-fold on binding to smS1 (data not shown) as seen previously for several other myosin heads [skS1 (*28*, *29*); *Dictyostelium* myosin II (*30*); scallop S1 (*31*); Ancanthaemeba myosin I (*32*)], and this provides a convenient signal to monitor the interaction of mantADP with S1 and acto·S1. As for the pyrene label on actin, the mant label reports the transition from the A- to R-state as the ADP changes from being tightly to weakly bound (see Scheme 4).

Most of the measurements made with ADP were repeated using mantADP. The rate of mantADP binding to S1 was similar to that of ADP, but the rate of displacement by ATP was approximately 10 fold slower, suggesting a 10-fold tighter binding of mantADP to smS1 (Table 2). This is similar to the result reported for skS1 and several other myosins. The experiment of Figure 4 was repeated using

mantADP in place of ADP and unlabeled actin in place of pyr-actin. The ATP-induced dissociation of actin from the complex was followed from the change in 90° light scattering using an excitation wavelength of 435 nm. As seen for ADP, the dissociation reaction was biphasic in the presence of mantADP (data not shown). The fast phase had a k_{obs} of 250 s^{-1} and a slow phase of 25 s^{-1}, and these rate constants were essentially independent of the concentration of mant·ADP. The total amplitude of the light scattering was independent of [mantADP], but the amplitudes of the slow phase increased and the fast phase decreased with a hyperbolic dependence on [mantADP]. Analysis of the curves was consistent with a K_d of 7 μM for mantADP binding to acto·S1, very similar to the affinity of ADP for acto.smS1 (Table 2). Thus, mantADP behaves in a similar way with both smS1 and skS1: it binds 10-fold tighter to both S1's than does ADP, due to a slower dissociation rate constant but binds to acto·S1 with a similar affinity to ADP.

Addition of 10 μM mantADP to 2 μM unlabeled actin and 1 μM S1 produced no change in mant fluorescence, yet subsequent addition of ATP demonstrated that mantADP was in the S1 binding site. Thus, the binding of mantADP to acto·smS1 causes no change in the mant fluorescence, and so the ternary complex is similar to the R-state identified for skS1 with the pyrene fluorescence quenched and the mant fluorescence similar to that for free ADP. The major difference to skS1 is that the affinities of both actin and ADP for the ternary complex are significantly tighter and no detectable A-state was present in the equilibrium mixture for smS1 compared to a 10% occupancy of this state for skS1.

DISCUSSION

It is of interest to compare our results (summarized in Tables 1 and 2) with those from previous studies of smS1. Marston and Taylor (*2*) under different conditions (pH 7, 20 °C, ~0.017 M ionic strength) characterized a similar form of gizzard myosin S1 made by digestion with papain which partially cleaves the regulatory light chain. Our measurements of the rates of ATP binding to smS1, of the ATP cleavage step (Figure 1), of ADP release from smS1·ADP (Figure 2), of dissociation of acto·smS1 by ATP (Figure 3), and of ADP release from acto·S1 are in general agreement with this earlier study. The rate of ADP release from the acto·S1 complex was reported by Siemankowski et al. (*4*) to be 15 s^{-1}, the same value reported by Marston and Taylor (*2*) at low ionic strength and a little lower than our value of 22 s^{-1} (Figure 4). The affinity of papain smS1 for actin in the absence of nucleotide has been estimated using a competition assay with skeletal S1 at 25 °C (*10*). Their values were 14 and 3.3 nM at ionic strengths of 0.23 and 0.05 M, respectively. These values are in reasonable agreement with the value measured here (17 nM and 3.5 nM at 0.22 and 0.12 M ionic strength) for *Staphylococcus* smS1.

Overall, smS1 behaves much like the well-studied skS1 except the ATP hydrolysis rate and ATP-induced dissociation of acto·S1 are 30−50% of the skS1 values. Perhaps more significantly, the binding of ADP to smS1 is very similar to skS1 in both rate and equilibrium constants, yet ADP binding to acto·smS1 is very different; the affinity is 20 times tighter and the dissociation rate constant is more than 20 times slower for smS1 than for skS1. This results in a marked difference in the coupling between nucleotide and actin binding to S1 (see Scheme 3). Table 2 lists the rate and equilibrium constants defined here for ADP and actin binding to smS1. In Table 3, the thermodynamic coupling of ADP and actin binding and the acceleration of ADP release by actin are compared with those of three other myosin heads. The details of how the binding of the two ligands is coupled and how this differs between myosins reveal information about the communication between the two binding sites through the S1 structure and about the adaptation of each myosin for its particular function.

Both actin and ADP reduce each other's affinity for S1; by a factor of ~5 for smS1, a factor of ~50 for skS1, and factors of 20 and 3 for the cardiac and *Dictyostelium* proteins. In the case of smS1, ADP reduces the affinity of actin for S1 by reducing the association rate constant (5-fold) with little effect on the dissociation rate constant. In contrast, actin accelerates both the ADP dissociation rate constant (11-fold) and the association rate constant (4-fold). A similar situation was observed for the ternary complexes with skS1 where ADP primarily reduced the actin association rate constant but actin accelerated both ADP release (>100-fold) and the rate of ADP binding [~4-fold (*25*)]. The other two myosin heads have not been defined in such detail. The change in thermodynamic coupling was pointed out previously for the *Dictyostelium* and rabbit fast myosins (*30*) and probably reflects different physiological roles of the myosins. However, the exact contribution of the actin-induced acceleration of ADP release and the coupling of the two affinities to physiological function remains ill-defined.

White and co-workers (*4*) were the first to point out the importance of ADP release in muscle contraction, showing that there was a correlation between the maximum rate of ADP release and the maximum shortening velocity for a wide range of muscle fiber types. More recently the off-rate of ADP from actomyosin−ADP in muscle fibers was shown to be correlated to the kinetics of relaxation for different types of smooth muscle tissue, tonic versus phasic (*33*). These and other data have led to the idea that ADP release plays an important role in determining the lifetime of the force-generating states and more recently that strain-dependent release of ADP would be one way of coupling the ATPase cycling rate with the speed of shortening [e.g. (*34*−*36*)]. However, the data in Table 2 suggest that at least two different types of behavior may be important in different myosins. In the faster striated muscles (skeletal and cardiac), there is a large acceleration of ADP release (>100) and a large thermodynamic coupling (>10). In the slower myosins (smooth and *Dictyostelium*), both the acceleration and thermodynamic coupling are lower. However, the actual affinities of ADP for acto·S1 do not fit into the same categories. The affinity of ADP for acto·S1 is tight (5 μM) for smooth and cardiac compared to the probable cellular concentration of ADP (see below). In contrast the affinity of ADP for skeletal and *Dictyostelium* acto·S1 is weak (100 μM). This suggests that in the case of smooth and cardiac actomyosin the system has to do work to displace ADP.

To interpret the role of the ADP release steps in a contracting muscle, the cellular ADP and ATP concentrations must be known as these determine the maximum effective

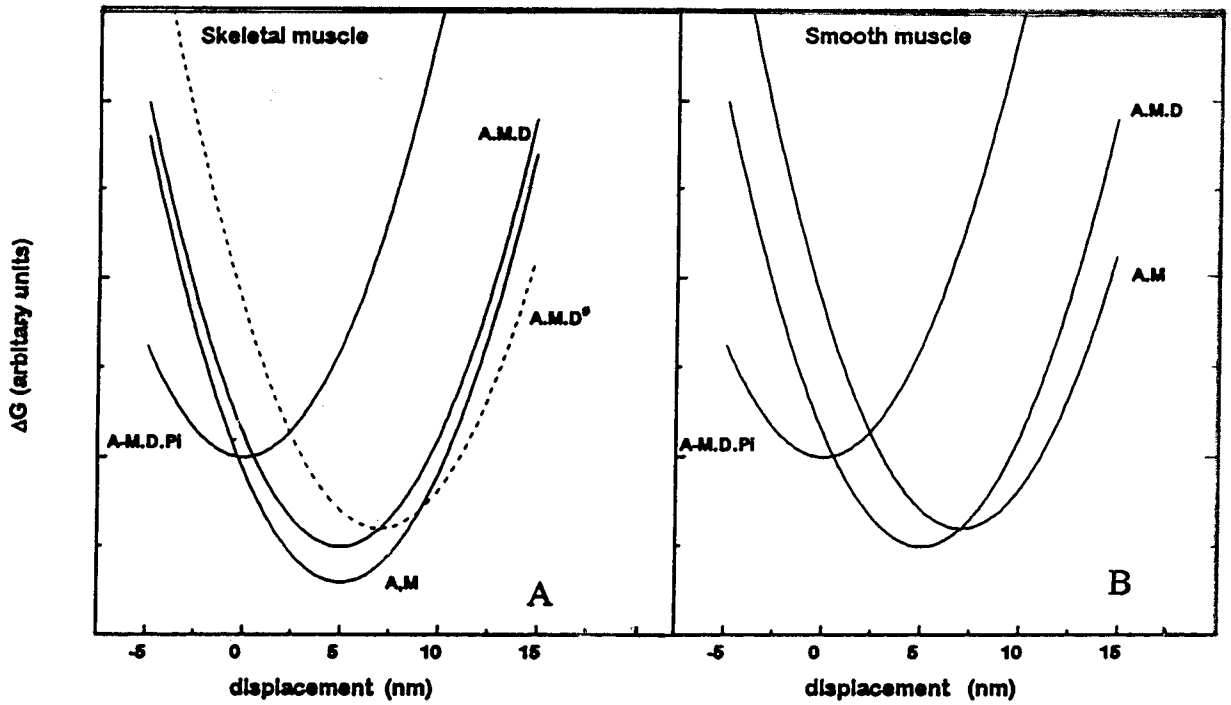

FIGURE 7: Proposed free energy diagrams for attached smooth and skeletal myosin crossbridges. The diagram shows the parabolic free energy diagrams for elastically distorted myosin crossbridges based on those of Hill (*39*). The following biochemically defined pathway is illustrated: A−M·D·P_i (the preforce attached or A-state), loss of phosphate to form A·M·D (more strongly attached rotated or rigor-like, R-state), loss of ADP to form A·M (also an R-state). (A) Skeletal muscle. The position of the minimum ΔG value for the preforce generating attached or A-state (A−M·D·P_i) is set arbitarily to zero, and the mimimum for the postforce R-state (A·M·D) is displaced by +5 nm, the crossbridge throw. This produces a positive strain on the crossbridge which can result in sliding of the two filaments. Loss of ADP from A·M·D to A·M changes the value of the minimum ΔG but not its position. The dotted line shows the relative position of the transition state A·M·$D^{\#}$ proposed by Smith and Geeves (*36*) that occurs on the pathway for ADP release from A·M·D. (B) Smooth muscle. The A−M·D·P and A·M·D states are shown as being identical to the corresponding states in skeletal muscle with the AM state at a higher ΔG and shifted to the right (see text).

rate of detachment of the crossbridge at the end of the power stroke and the free energy change associated with ADP release. The ADP concentration has not been unequivocally determined for smooth muscles, but all estimates suggest that it is greater (20 μM) or much greater (100 μM) than the K_D for ADP binding to acto·S1 [see (*37*) and references within]. If the measurements for S1 in solution reflect the situation in the muscle, then there is an energetic cost of ADP release. In the normal full crossbridge cycle, this is not a problem as the following ATP binding step will drive the reaction in the forward direction.

The ADP-induced structural change in smooth acto·S1 observed by Whittaker et al. (*6*) and confirmed by the EPR (*8*) and X-ray data (*9*) is unlikely to be a force-generating mechanism if it requires energy. Yet the EPR study showed that the effect of ADP was both reversible and saturable, allowing an estimate of the affinity for ADP of 5 μM. This is in good agreement with our solution measurement of K_{AD} (Table 2) and with the value estimated by Poole et al. (*9*) using X-ray fiber diffraction. Furthermore, estimates of ADP affinity for rigor crossbridges in phasic and tonic smooth muscle (from the ADP inhibition of the rates of relaxation of rigor fibers) show a similar high affinity (*38*). However, no such measurements have been made with chicken gizzard muscle fibers. These studies together suggest that the affinity of ADP for the crossbridge is high compared to the free concentration of ADP in smooth muscle. And therefore on thermodynamic grounds the structural change induced on ADP release is unlikely to be a source of additional force transduction compared to the skeletal myosin. Other possible roles for the ADP effect were discussed by Barsotti et al. (*7*), who suggested a role in myosin regulation or in controlling ADP release from the latch state.

The crossbridge free energy diagrams developed by Hill (*39*) are helpful in an interpretation of the role of ADP in the structural and free energy changes in the crossbridge cycle. Figure 7A shows the parabolic free energy diagrams for attached crossbridges in the A- and R-states for the familiar skeletal system. In this model, the minimal free energies for the A·M·D and A·M R-states are at the same position and displaced by +5 nm (the crossbridge throw) from the position of the minimal free energy of the preforce attached A-state (A−M·D·P). In this form, strain on the crossbridge imposes no restriction for ADP release. This has always posed problems for an efficient crossbridge cycle as ideally the ADP release (and hence ATP binding and crossbridge detachment) should not occur until the end of the power stroke and shortening has occurred. This would give rise to the Fenn effect (*40*).

There is little direct evidence for strain-dependent ADP release, i.e., crossbridges bearing positive strain having a longer lifetime than crossbridges bearing zero or negative strain. Yet most crossbridge models require such a mechanism to be introduced. Smith and Geeves (*36*) proposed the transition state, A·M·$D^{\#}$, between A·M·D and A·M, shown in dotted lines in Figure 7A, to account for such

phenomena. This was rationalized as a thermally induced opening of the ADP pocket to allow ADP release, and the opening of the pocket was opposed by strain on the head. As this is a transition state, it provides an effect of strain on the rate of the A·M·D to A·M transition but not on its equilibrium constant.

A similar free energy diagram for smooth muscle is shown in Figure 7B which incorporates the new structural information. The proposed A·M state has its minimum ΔG value at +2.5 nm further displacement from A·M·D (which is similar to both A·M and A·M·D in the skeletal system), and the minimum free energy value of A·M is slightly higher than that of A·M·D. The figure shows that this smooth A·M state appears similar to the A·M·D$^{\#}$ transition state proposed for the skeletal crossbridge. It is clear that any A·M·D crossbridge bearing strain requires a large input of energy for ADP to be released. If this energy has to come from thermal sources, then this transition will be very unlikely while the head bears positive strain. As the strain is lowered by sliding of the filaments, the transition becomes accessible via thermal fluctuations, and at negative strains, ADP will be readily released. Such a model for smS1 therefore provides an effective strain-dependent ADP release mechanism with inhibition of ADP release for crossbridges bearing positive strain and enhanced ADP release at negative strains even in the presence of free ADP concentrations in excess of 5 μM.

This interpretation suggests that a high relative affinity of ADP for acto·S1 may be coupled to the ADP induced structural change in acto·S1 and the proposed strain limited ADP release mechanism. The data in Table 3 suggest that a structural change may be expected on ADP release in cardiac but not in *Dictyostelium* myosin. The data in Table 3 also provide information on how the four myosins are adapted for their individual functions. If the rate of ADP release from acto·S1 defines the lifetime of the attached crossbridge during high speeds of shortening, as first proposed by White and collaborators, it is related to the maximum shortening velocity for the myosin type. The thermodynamic coupling limits the extent to which ADP release can be accelerated by actin without consequences for other parts of the crossbridge cycle. Any increase in the rate of ADP release from acto·S1 will result in a reduction in the affinity of ADP for acto·S1(increase in K_{AD}), and the thermodynamic coupling requires a change in one or more of the other affinities in Scheme 3 ($K_{AD} = K_D K_{DA}/K_A$). A change in K_D may be undesirable as it is likely to affect the affinity of ATP for S1 and acto·S1. The alternative is either to strengthen the affinity of actin for S1 or to weaken the affinity of actin for S1·ADP or a combination of the two. A reduction in the affinity of actin for S1·ADP will be undesirable in a myosin which bears high loads (e.g., smooth myosin) but may be acceptable in a myosin designed for high velocities (e.g., skeletal myosin). Thus, differences in acceleration and thermodynamic coupling revealed in Table 3 are probably the result of optimizing the parameters available to each myosin by a combination of varying the three parameters: affinity of the crossbridge for ADP compared to the concentration of free ADP in the cell; the size of the structural change from A·M·D to A·M; and the degree of coupling between actin and nucleotide binding different myosins may be tuned to the physiological requirements. It will be of interest to compare the behavior of phasic and tonic smS1 and the behavior of a wide range of different myosins in terms of the coupling of ADP and actin binding and their structures as these become available.

ACKNOWLEDGMENT

We thank Nancy Adamek, Geetha Ramaprian, My-nuong Vo, and Dr. Xiangdong Wu for technical help with protein preparations and characterization, and Dr. Roger Goody for continual support.

REFERENCES

1. Somlyo, A. P., and Somlyo, A. V. (1994) *Nature 372*, 231−236.
2. Marston, S. B., and Taylor, E. W. (1980) *J. Mol. Biol. 139*, 573−600.
3. Guilford, W. H., Dupuis, D. E., Kennedy, G., Patlak, J. B., and Warshaw, D. M. (1997) *Biophys. J. 72*, 1006−1021.
4. Siemankowski, R. F., Wiseman, M. O., and White, H. D. (1985) *Proc. Natl. Acad. Sci. U.S.A. 82*, 658−662.
5. Barany, M. (1967) *J. Gen. Physiol. 50*, 197−216.
6. Whittaker, M., Wilson-Kubalek, E. M., Smith, J. E., Faust, L., Milligan, R. A., and Sweeney, H. L. (1995) *Nature 378*, 748−751.
7. Barsotti, R. J., Dantzig, J. A., and Goldman, Y. E. (1996) *Nat. Struct. Biol. 3*, 737−739.
8. Gollub, J., Cremo, C. R., and Cooke, R. (1996) *Nat. Struct. Biol. 3*, 796−802.
9. Poole, K. I. V., Lorenz, M., Ellison, P., Evans, G., Rosenbaum, G., Boesecke, P., Holmes, K. C., and Cremo, C. R. (1997) *J. Muscle Res. Cell Motil. 18*, 264.
10. Greene, L. E., Sellers, J. R., Eisenberg, E., and Adelstein, R. S. (1983) *Biochemistry 22*, 530−535.
11. Rosenfeld, S. S., Xing, J., Rener, B., Lebowitz, J. J., Kar, S., and Cheung, H. C. (1994) *J. Biol. Chem. 269*, 30187−30194.
12. Ikebe, M., and Hartshorne, D. J. (1985) *Biochemistry 24*, 2380−2387.
13. Ikebe, M., and Hartshorne, D. J. (1985) *J. Biol. Chem. 260*, 13146−13153.
14. Persechini, A., Kamm, K. E., and Stull, J. T. (1986) *J. Biol. Chem. 261*, 6293−6299.
15. Wells, J. A., Werber, M. M., Legg, J. I., and Yount, R. G. (1979) *Biochemistry 18*, 4793−4799.
16. Lehrer, S. S., and Kerwar, G. (1972) *Biochemistry 11*, 1211−1217.
17. Criddle, A. H., Geeves, M. A., and Jeffries, T. E. (1985) *Biochem. J. 232*, 343−349.
18. Hiratsuka, T. (1983) *Biochem. Biophys. Acta 742*, 496−500.
19. Bagshaw, C. R., Eccleston, J. E., Eckstein, F., Goody, R. S., Gutfreund, H., and Trentham, D. R. (1974) *Biochem. J. 141*, 351−364.
20. Millar, N. C., and Geeves, M. A. (1983) *FEBS Lett. 140*, 11−15.
21. Siemankowski, R. F., and White, H. D. (1984) *J. Biol. Chem. 259*, 5045−5053.
22. Geeves, M. A., and Conibear, P. B. (1995) *Biophys. J. 68*, 194−201s.
23. Geeves, M. A. (1991) *Biochem. J. 274*, 1−14.
24. Millar, N. C., and Geeves, M. A. (1988) *Biochem. J. 249*, 735−743.
25. Geeves, M. A. (1989) *Biochemistry 28*, 5864−5871.
26. Geeves, M. A., and Jeffries, T. E. (1988) *Biochem. J. 249*, 735−743.
27. Kurzawa, S. E., and Geeves, M. A. (1996) *J. Muscle Res. Cell Motil. 17*, 669−676.
28. Woodward, S. K. A., Eccleston, J. F., and Geeves, M. A. (1991) *Biochemistry 30*, 422−430.
29. Cremo, C. R., Neuron, J. M., and Yount, R. G. (1990) *Biochemistry 29*, 3309−3319.

30. Ritchie, M. D., Geeves, M. A., Woodward, S. K. A., and Manstein, D. J. (1993) *Proc. Natl. Acad. Sci. U.S.A. 90*, 8619−8623.
31. Perreault, C. L., Trybus, K. M., Geeves, M. A., Kurzawa, S., and SzentGyorgyi, A. G. (1997) *Biophys. J. 72*, A180.
32. Ostap, E. M., and Pollard, T. D. (1996) *J. Cell Biol. 132*, 1053−1060.
33. Khromov, A. S. (1996) *J. Physiol. 492.3*, 669−673.
34. Hibberd, M. G., and Trentham, D. R. (1986) *Annu. Rev. Biophys. Biophys Chem. 15*, 119−161.
35. Cooke, R., White, H., and Pate, E. (1994) *Biophys. J. 66*, 778−788.
36. Smith, D. A., and Geeves, M. A. (1995) *Biophys. J. 69*, 524−537.
37. Clark, J. F., Kemp, G. J., and Radda, G. K. (1995) *J. Theor. Biol. 173*, 207−211.
38. Fuglsang, A., Khromov, A., Torok, K., Somylo, A. V., and Somylo, A. P. (1993) *J. Muscle Res. Cell Motil. 14*, 666−673.
39. Hill, T. L. (1974) *Prog. Biophys. Mol. Biol. 28*, 267−340.
40. Fenn, W. O. (1923) *J. Physiol. 58*, 175−203.

BI9722406